Exploration Geophysics 2025, 56 no. 5: 44–55 doi:10.63929/08123985.2025.56.03

Analysing the invisible: GPR survey at the Church of the Holy Sepulchre in Jerusalem

V. Di Fiore[a], M. Punzo[a], I. Ferrari[b], L. De Giorgi[b], F. Giuri[b], D. Tarallo[a], P. Croveri[c], M. Cardinali[c] and G. Leucci[b*]

[a] Institute of Heritage Sciences, National Research Council, 80133 Napoli, Italy; [b] Institute of Heritage Sciences, National Research Council, 73100 Lecce, Italy; [c] Centro per la Conservazione ed il Restauro 'La Venaria Reale', 10078 Venaria Reale (TO), Italy

ABSTRACT

The Church of the Holy Sepulchre in Jerusalem, undoubtedly the symbol par excellence of Christianity, is the primary Christian pilgrimage destination since its creation in the fourth century. It has preserved its historical, religious, cultural, tangible and intangible values until today. Being a 'Living Religious Heritage' under the custody of the Christian communities, the Church underwent several transformations over the centuries following historical, natural and accidental events, leading to the current structure of the Basilica. At the beginning of the third millennium, planning for restoration interventions was set out by the Christian communities; initially, renovation of the *aedicule* (the Tomb of Christ). Subsequently, a feasibility study aimed at restoration of the entire floor of the Church was carried out by an interdisciplinary team that planned technical and scientific surveys to document the present state of the floor and the underground situation. Some geophysical surveys were undertaken on the shared spaces per the status quo rules to investigate the presence of buried archaeological structures and more recent technical facilities. The ground penetrating radar (GPR) method was used with good results for the depth of bedrock under the floor, thickness of the ashlars, the presence of ancient buried structures and cavities (channels, walls, and paving roads), and the water contents of the soil layers. These are visualised in 3D virtual excavations.

Key words: ground penetrating radar, Holy Sepulchre, Jerusalem, virtual excavation.

INTRODUCTION

The study and preservation of historical sites and built cultural heritage monuments are a focus of significant efforts for the scientific community. In the past, actions related to the study, conservation, and relative protection of the built cultural heritage were based on the application of inadequate methodologies associated with the available technological resources (Leucci, 2019). This approach, which involved the application of an initial visual inspection and subsequently (to investigate more in-depth) destructive investigations such as sampling, core drilling, and excavation (Leucci, 2019), limited the effectiveness of the restoration interventions and could be the cause, in some cases, of damage to the investigated built cultural heritage. Non-destructive techniques are indispensable in built cultural heritage (Leucci, 2019). They allow the detection of the degree of deterioration at several depths and investigation of buried structures inside the studied monument. Often, non-destructive techniques are related to the applications of geophysical methods. In the field of the study of the conservation state of built cultural heritage, the international literature shows several applications of geophysical methods (Leucci et al., 2007; Moropoulou et al., 2012; Leucci, 2019; Leucci and De Giorgi, 2022; De Giorgi et al., 2023a, b; Riminesi et al., 2024; Tanasi et al., 2023).

The basilica of the Holy Sepulchre, under the custody of the Christian communities, is undoubtedly the symbol par excellence of Christianity and has a universal value: its religious, cultural and historical value is so exceptional that it transcends national borders and takes on absolute importance for present and future generations of all humanity. Moreover, the Church of the Anastasis (Church of the Holy Sepulchre) is considered as a 'Living Religious Heritage' not only because millions of pilgrims and tourists visit it every year, but also because the Christians communities lodge in the canonical spaces and celebrate the historical liturgies daily, following the 'status quo' regulations, handed down as rituals from one generation to another.

In this sense, every effort in planning a restoration intervention of this historical and religious monument must go beyond the mere conservation practice of monumental heritage oriented towards the preservation of materials, giving space and attention to the intangible and relational values connected to the communities that are part of it.

Following this methodological approach, the Centro per la Conservazione ed il Restauro dei Beni Culturali La Venaria Reale was entrusted by the three main Christian communities (the Greek Orthodox Patriarchate of Jerusalem, the Custody of the Holy Land, the Armenian Patriarchate of Jerusalem) to plan a conservation intervention of the entire stone floor of the common spaces of the Church of Holy Sepulchre with the

* Email: giovanni.leucci@cnr.it

© The Author(s) 2025. Published by the ASEG. All rights reserved until 1 February 2026. After that date, excluding any third-party material, the details of which are cited in the references, this article is licenced: CC BY-NC-ND 4.0 (https://creativecommons.org/licenses/by-nc-nd/4.0/).

collaboration of an interdisciplinary team of experts and in parallel with the archaeological excavations led by of the Sapienza University of Rome.

Preliminary scientific investigations and methods were applied to investigate the state of conservation, document the current conditions, and collect all the necessary data to perform a feasibility study and correctly design the intervention phase. The Department of Architecture, Built Environment and Construction Engineering of the Politecnico di Milano developed an Historical Building Information Modelling (HBIM) system to store FAIR data starting from the 3D acquisitions of the pavement. At the same time, the Institute of Heritage Science of the Italian National Research Council (CNR-ISPC) conducted some geochemical analysis on materials and a complete ground penetrating radar (GPR) survey of the floor areas. This work focuses on the use of GPR and digital images to support the planning of the conservation interventions on a significant monument, the Holy Sepulchre Church in Jerusalem (Figure 1). A part of the Church was previously investigated with the aim of the characterization of materials, and detection of wear and degradation of materials in the part of the Church surrounding the *aedicula* (Kyriakos and Moropoulou, 2013; Moropoulou et al., 2013, 2018; Kyriakos et al., 2017; Alexakis et al., 2018). The GPR inspection aimed to expand knowledge about the presence of buried structures of archaeological interest, identify the depth of the bedrock (the so-called sacred rock), identify the thickness of the ashlars that form the flooring of the church, and determine the volumetric water content on the surface.

The results, shown in terms of virtual excavation thanks to digital images, reveal several buried secrets.

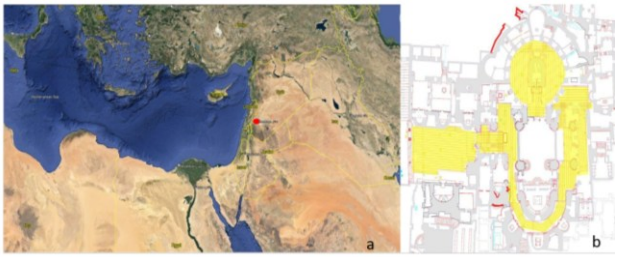

Figure 1. a) Location (from Google Earth) of the city of Jerusalem (Israel). b) Map of the Church of the Holy Sepulchre; in yellow are highlighted the investigated areas.

HISTORICAL SETTING

The Church of the Holy Sepulchre is considered the most important church in Christendom. Unveiling its complex and centuries-old history is a continuous and multifaceted challenge that historians and researchers have faced, and will continue to face in the future.

The church structure underwent several modifications in ancient times due to historical events, catastrophic natural and anthropogenic events, construction, renovation and maintenance interventions conducted by the religious communities living continuously inside the premises. The most significant events, relevant to the present study, focused on the floor and the underground layers, are summarised in Table 1.

Retrieval of information about the various construction phases and transformations of the floor and the underground stratigraphy was carried out in particular by Father Corbo, between the 1960s and the 1980s, through archaeological studies and wide-ranging excavations in several areas of the Church (Corbo,1981). The most recent studies on the transformations of the subsurface of the entire basilica were carried out by the University of Florence (Garbarino et al., 2019).

Moreover, insights on the underground conditions were provided on the occasion of the restoration of the Tomb of Christ (the holy *aedicula*) in 2016–2017, when the National Technical University of Athens (NTUA) performed a GPR survey in the Anastasis Rotunda area (Lampropoulous et al., 2017; Moropoulou, 2013, 2017).

Table 1. The most significant events impacting the floor of the Holy Sepulchre Church (Tucci, 2019).

Years AD	Most significant events
135	Emperor Hadrian orders the construction of a temple
326	Construction of the basilica ordered by Constantine begins
335	Dedication of Constantine's basilica
614	The Persians set fire to the basilica
634–38	Modestus orders the restoration of the building.
800	An earthquake destroys the Anastasis dome
815–966	Decline of Sanctuary, owing to fires and pillaging
1009	Caliph al-Hakim orders the destruction of the complex
1042–48	Emperor Constantine Monomachus orders the reconstruction of the basilica, partly altering its layout
1130–49	The Crusaders continue the reconstruction of the Sanctuary
1188	Beginning of decline: Saladin closes to worship
1246	The keys are entrusted to Muslim families
1545	An earthquake destroys a part of the bell tower
1555	Consolidation work by the Franciscans on the *aedicule* and the dome
1808	Fire in the basilica
1810–37	Parts of the building were shored up, and rather rough-and-ready renovation work (architect: Komnenos[†])
1867	An earthquake damaged the Anastasis dome, and it was renovated in metal (architect: Mauss[‡])
1927	An earthquake damages the complex
1934	The Public Works Department of the British Mandatory shored up all building parts
1947	Installation of containment and reinforced structures by the Public Works Department of the British Mandatory
1960	Start of restoration work commissioned by all Christian communities, archaeological excavations by Father Corbo
1997	Restoration of the Anastasis dome and washroom areas
2016–17	Restoration of the Shrine of the Tomb of Christ (National Technical University of Athens)

[†] The architect Nikolaos Komnenos (1770–1821), a Mytilene native, worked at the Holy Sepulchre from May 3rd 1809, the date on which he left Istanbul for this assignment, until September 13th 1810 (Biddle, 2000a).

[‡] Heinrich Friedrich August Mauss (1839–1917) was a German architect known for his work on historical buildings, including restorations and new constructions in Germany and Italy.

GEOLOGICAL SETTING

Jerusalem, located approximately 760 m above sea level, is on the mountainous ridge of Israel, corresponding to the main watershed between the Mediterranean and the Dead Sea. The lithostratigraphic sequence is commonly characterised by a thick (900–1000 m) sequence of hard and permeable limestone and dolomite, interbedded with clayey impermeable layers (late Cretaceous). The overlying sediments (Senonian–Maastrichtian) are characterised by a thick sequence of homogeneous chalk and marls (Shtober-Zisu and Zissu, 2018). In particular, the church is situated on the Shivta Formation (Bentor and Vroman, 1963; Type Section: Arkin and Braun, 1965) (Figure 2), comprising predominantly limestone (Turonian, thickness 20–40 m).

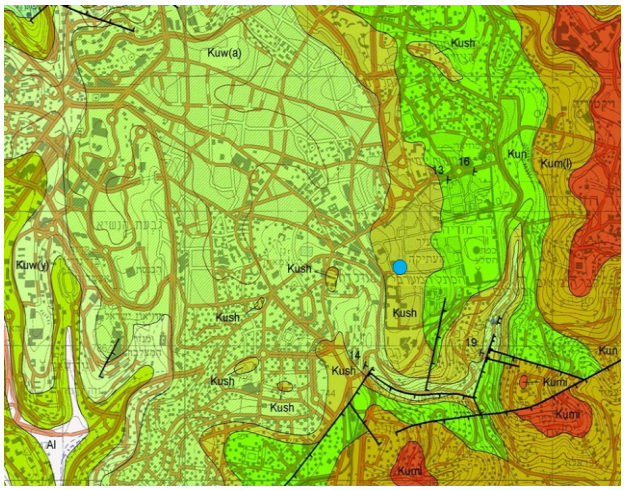

Figure 2. Geological map of Israel 1:50.000 (Jerusalem sheet 11-II, Ministry of National Infrastructures, Earth and Marine Research Administration, 2001). The blue dot identifies the Church of the Holy Sepulchre. LEGEND: Kuw(y): dolomite (upper Cenomanian, thickness 30 m); Kuw(a): dolomite (lower Turonian; thickness 35 m); Kush: limestone (middle Turonian, thickness 20–40 m); Kun: limestone with sand and marl (upper Turonian, thickness 40–90 m); Kum(I): chalk (Santonian, thickness 60–100 m); Kum(u): chalk (lower Campanian, thickness 0–90 m); Kumi: Chert (upper Campanian, thickness 90 m); Blue lines are the geological structures.

The Shivta Formation crops out mainly south of Jerusalem city. It includes two members: a lower member and and upper member. The lower member, of dark-grey limey dolomite 0–20 m thick, is found along the eastern and southeastern margins of the Auja Monocline and thins out westward. The upper member comprises two lithologic types: biomicrite or pelbiomicrite, mud supported, and biosparite or pelbiosparite, mud supported or grain supported. Bioclasts of the latter type are well rounded. Lenses of quartzolite – a very rare, coarse-grained intrusive igneous rock in which quartz makes up more than 90% of the felsic mineral content – up to 40 cm thick are present at the top of the Shivta Formation (Begin, 1974). The Shivta Formation forms a typical cliff morphology with many caves. The dolomite has a dark-grey patina, whereas the limestone is light grey (Begin, 1974).

The city of Jerusalem has grown for ~4,000 years on karst terrain. The surface topography lacks closed depressions, but karst is well demonstrated by speleology and subsurface hydrology. Several caves in the city were truncated by construction works, including an 800 m-long river cave (the longest limestone river cave in Israel). Caves are increasingly being discovered, as construction works dig deeper into the subsurface of the crowded city. The construction works have eventually destroyed some of them. The hydrogeology of the Gihon, Jerusalem's main karst spring, was studied to understand its behaviour and the effects of urbanisation on karst groundwater resources. High-resolution monitoring of the spring discharge, temperature and electrical conductivity, and chemical and bacterial analysis, demonstrate a rapid response of the spring to rainfall events and human impact. A complex karst system is inferred, including conduit, fissure, and diffuse flow (Frumkin 2013).

MATERIALS AND METHODS

The success of GPR surveys mainly depends on soil and sediment mineralogy, clay content, ground moisture, burial depth, surface topography, and vegetation (Conyers, 2004; Leucci 2008, 2015, 2019). It is not a geophysical method that can be immediately applied to any geographic or archaeological setting. However, with thoughtful acquisition and data processing methodology modifications, GPR can be adapted to many site conditions. Most GPR practitioners have assumed that the method would only be successful in areas where soils and underlying sediment are dry (Annan and Davis 1978). Although radar wave penetration and the ability to reflect energy to the surface are often enhanced in a dry environment, recent work has demonstrated that dryness is not necessarily a prerequisite for GPR surveys, and even very wet environments are suitable, as long as the medium is not electrically conductive (Conyers 2004).

The GPR method involves the transmission of high-frequency electromagnetic radio (radar) pulses into the earth and measuring the time elapsed between transmission, the reflection from a buried discontinuity, and reception back at a surface radar antenna. A pulse of radar energy is generated on a dipole transmitting antenna placed on or near the ground surface. The resulting wave of electromagnetic energy propagates downward into the ground where some energy can be reflected to the surface from discontinuities.

The discontinuities where reflections occur are usually created by changes in the electrical properties of the sediment or soil, lithological changes, differences in bulk density at stratigraphic interfaces and, most crucially, water content variations. Reflection can also occur at interfaces between anomalous archaeological features and the surrounding soil or sediment. Void spaces in the ground, encountered in burials, tombs or tunnels, will also generate significant radar reflections due to a considerable change in radar wave velocity. The depth to which radar energy can penetrate and the amount of definition expected in the subsurface are partially controlled by the frequency of the radar energy transmitted. Radar energy frequency controls both the wavelength of the propagating wave and the amount of weakening, or attenuation, of the waves in the ground.

Analysing the spatial distribution of the amplitudes of reflected waves is important because it indicates subsurface changes in lithology and other physical properties. The higher the contrasting velocity at a buried interface, the greater the reflected wave amplitude. If amplitude changes can be related to important buried features and stratigraphy, the location of higher or lower amplitudes at specific depths can be used to reconstruct the subsurface in three dimensions. Areas of low-amplitude waves indicate uniform matrix material or soils, while those of high amplitude denote areas of high subsurface contrast, such as buried archaeological features, voids or important stratigraphic changes.

To be correctly interpreted, amplitude differences must be analysed in discrete slices that examine only the strength of reflections within specific depths in the ground. Each slice consists of the spatial distribution of all reflected wave amplitudes at various depths, indicative of these changes in

sediments, soils and buried materials. Amplitude slices need not be constructed horizontally or even in equal time intervals. Depending on the question being addressed, they can vary in thickness and orientation (Conyers and Goodman, 1997). To compute horizontal amplitude slices, the computer compares amplitude variations within traces recorded within a defined time window (that can become depth windows if velocities are known). When this is done, both positive and negative amplitudes of reflections are compared to the norm of all amplitudes within that window. No differentiation is usually made between positive and negative amplitudes in these analyses; only the magnitude of amplitude deviation from the norm is considered. Low-amplitude variations within any slice denote little subsurface reflection, indicating relatively homogeneous material. High-amplitude variations indicate significant subsurface discontinuities, which, in many cases, detect the presence of buried features.

Using 3D GPR reflection data, buried features can be rendered into isosurface images, meaning that the interfaces producing the reflections are placed in a 3D picture, and a pattern or colour is assigned to specific amplitudes for them to be visible (Leckebusch, 2003; Conyers, 2004; Goodman et al., 2004). Typical amplitudes (usually the highest) in programs that produce these images can be patterned or coloured, while others are transparent. To simulate sunlight, computer-generated light sources can then shade and shadow the rendered features to enhance them. The elements can be rotated and shaded until the desired image results.

The GPR data were collected using the Sir 3000 georadar system (GSSI), which used 270 MHz and 900 MHz antennas along grids with parallel profiles set 0.4 m apart for the 270 MHz and 0.2 m apart for the 900 MHz (Figure 3). The surveyed zone was divided into five main areas (Figure 4).

GPR data were processed using GPRslice software [GPR-SLICE 7.0 Download - gprslicev7.exe (informer.com)]. In order to eliminate a small noise component and make it easy to interpret the GPR data, the following processing sequence was applied (Giannino and Leucci, 2021):

1. zero-time adjust (static shift), in order to associate zero-time with zero-depth
2. frequency filtering used to remove high-frequency noise
3. migration to correct the shape and dimension of reflection events related to the structure present in the subsoil.

Figure 3. Phases of GPR data acquisition.

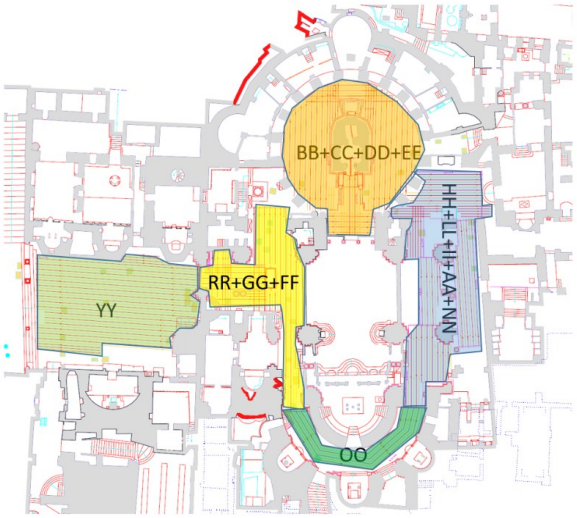

Figure 4. Areas surveyed using a 270 MHz antenna.

GPR DATA ANALYSIS AND RESULTS

Area BB+CC+DD+EE

In the area BB+CC+DD+EE (Figure 4), 70 GPR profiles were acquired using the 270 MHz antenna (Figure 5).

The reflection event evidenced by a dashed yellow line (labelled B) is probably related to the bedrock, which ranges from about 1.2 to 2.8 m deep. The T reflection events are related to the maintenance holes visible on the surface. The reflection events labelled C at a depth of about 0.1–0.3 m are related to known cavities. Inside the cavity C (already known), some metal structures (M) supporting the roof are visible.

Some reflection events labelled V at a depth between 0.9 and 1.1 m in the radar sections 5, 6 and 7 (Figure 5) are probably related to a void space. Also, the reflection events labelled V at a depth between 1.7 and 2.0 m (Figure 5) are likely associated with void spaces. Here, it is possible to note a change in the polarity of the electromagnetic wave (Conyers, 2015). These anomalies have a low reflection amplitude because they could be a partial presence of incoherent materials. Archaeologists report some channels of terracotta material covered in crushed bricks in this zone. The reflection event labelled 'A' visible at 1.9–2.0 m in depth could be related to traces of cart tracks.

In Figure 6, the reflection event evidenced by a dashed yellow line (labelled B1) is probably related to the first level of the bedrock. Its depth ranges from about 0.2 to 0.6 m. It is also possible to pick the bedrock's second level (B2). Its depth ranges from 1.4 to 1.7 m. The first bedrock level (B1) shows greater homogeneity than the second level B2. The second level, B2, offers a strong subhorizontal stratification. (Figure 6).

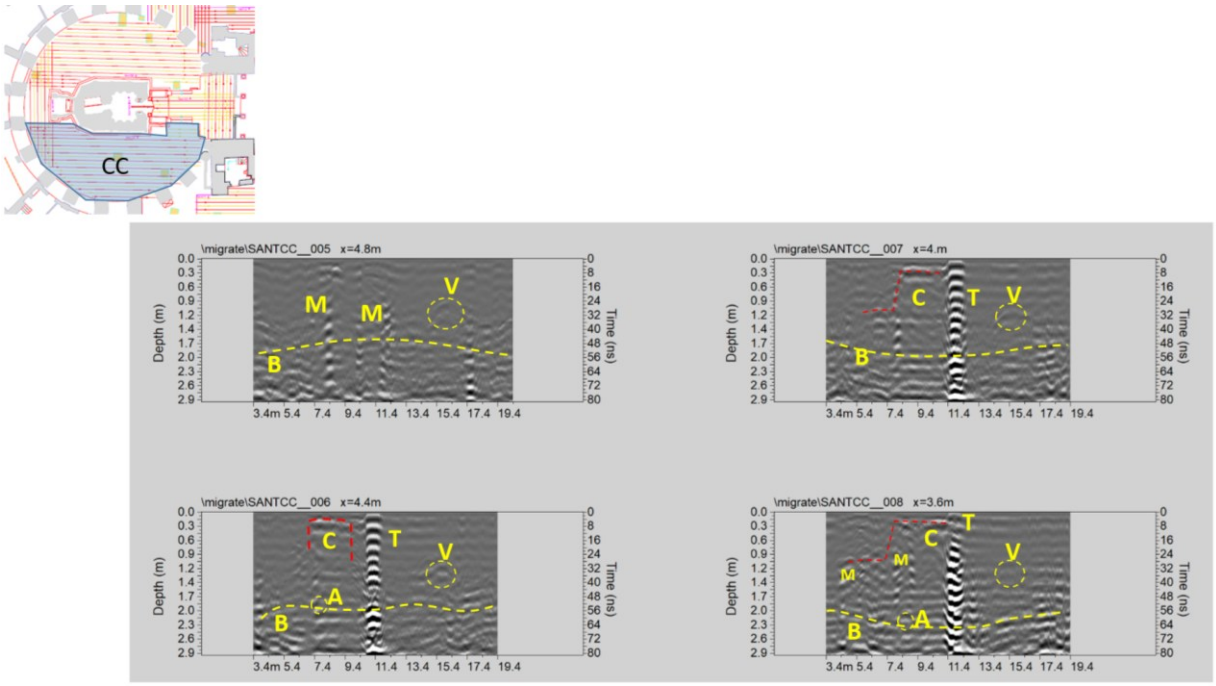

Figure 5. Area CC: Processed GPR profiles (A: traces of cart tracks; T: maintenance hole; C: Cavity; M: metal object; B: bedrock; V: void space).

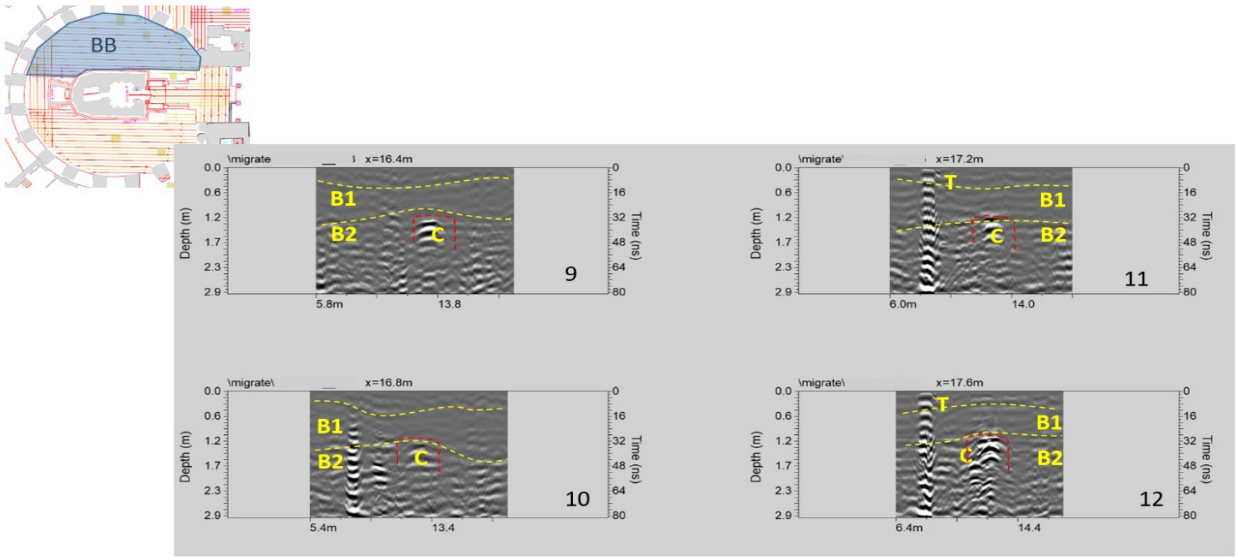

Figure 6. Area BB: Processed GPR profiles (C: cavity; B1: first level of bedrock; B2: second level of bedrock).

For the area DD, the reflection event evidenced by a dashed yellow line (labelled B) is probably related to the bedrock level. Its depth ranges from about 0.2 to 0.6 m. The reflection events labelled 'V1' and 'V2' are probably associated with the void spaces at depths between 0.6 and 0.7 m (V1) and 1.2 and 1.5 m (V2; Figure 7).

For the area EE, the reflection event evidenced by a dashed yellow line (labelled B) is probably related to the bedrock level. Its depth ranges from about 0.2 to 0.8 m. The reflection events labelled C are probably associated with a cavity 1.7 and 2.2 m deep. The reflection events labelled 'T' are due to a maintenance hole visible on the living surface (Figure 8).

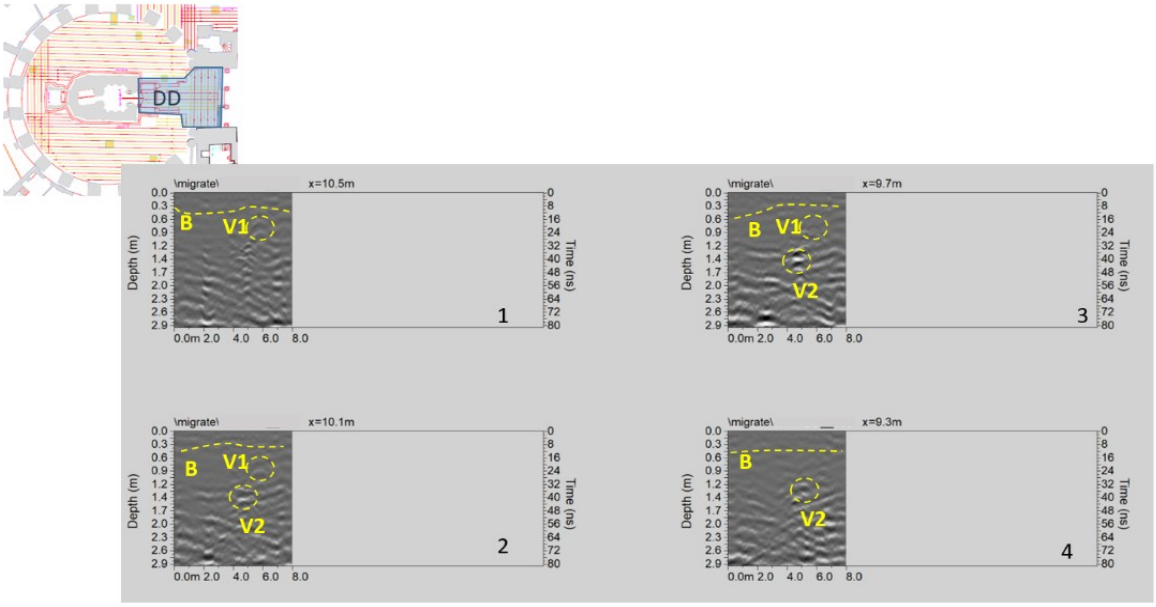

Figure 7. Area DD: Processed GPR profiles. B: bedrock; V1 and V2: void spaces.

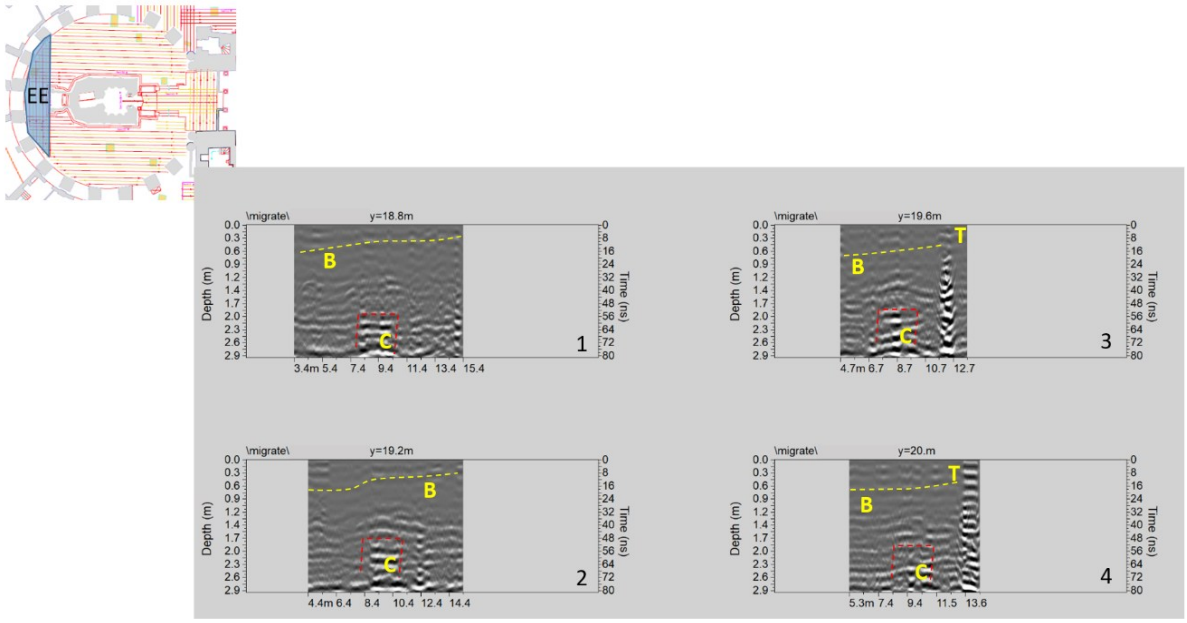

Figure 8. Area EE: Processed GPR profiles (B: bedrock; C: cavity; T: maintenance hole).

A way of obtaining visually useful maps for understanding the plan distribution of reflection amplitudes within specific time intervals is the creation of horizontal time slices. These are maps on which the reflection amplitudes have been projected at a specified time (or depth) with a selected time interval (Conyers, 2006). In a graphic method developed by Goodman et al. (2006), termed 'overlay analysis', the strongest and weakest reflectors at a depth of each slice are assigned specific colours. This technique allows the linkage of structures buried at different depths. This represents an improvement in imaging because subtle features indistinguishable on radargrams can be seen and interpreted more easily. The present paper uses the time-slice technique to display the amplitude variations within consecutive time windows of width $\Delta t = 5$ ns. Time (or depth) slices can be seen as a virtual excavation that places the interesting structures at their depth.

The time slices show the amplitude using a range defined by blue as zero and red as the maximum value. Figure 9 shows the depth slices from 0.1 to 2.9 m.

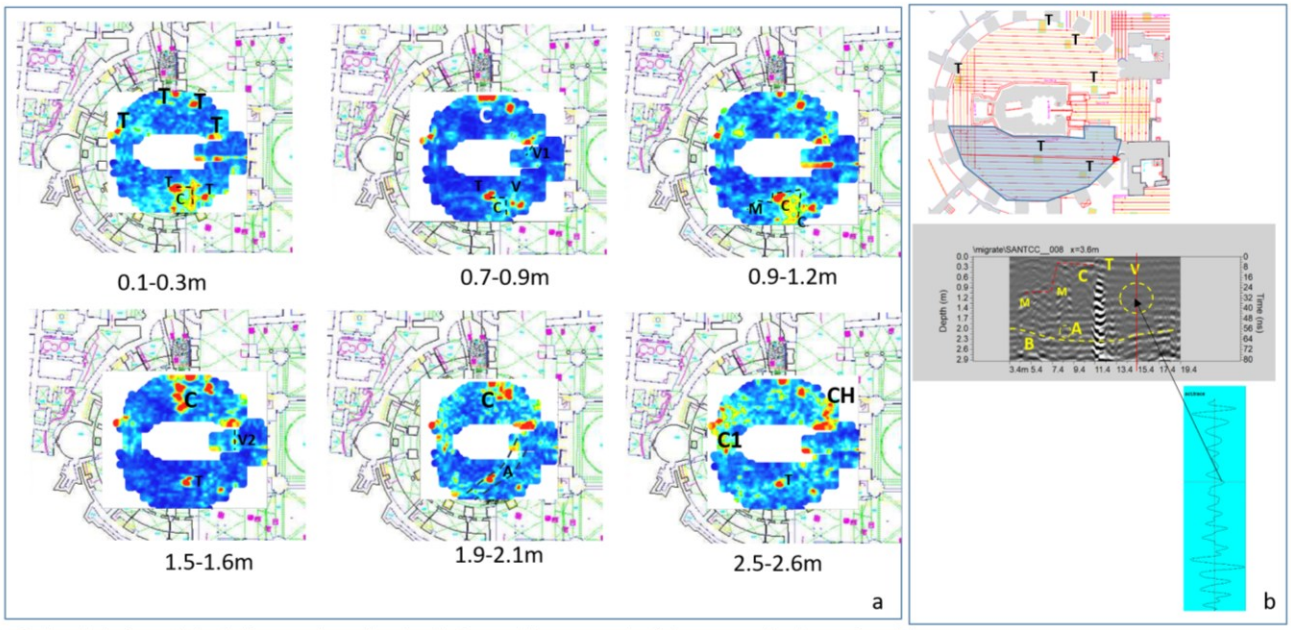

Figure 9. The whole area: (a) Depth slices overlapped to the planimetry depth slices (C: known cavity; C1 unknown cavity; A: traces of cart tracks; CH: channel; M: metal object; V, V1 and V2: void spaces; T: maintenance hole. (b) An exsample of the processed radar section with an indication of the anomalies and the change of the polarity related to the anomaly V

The high-amplitude anomalies (labelled C) in the time slices (Figure 9a) ranging from 0.1 to 1.5 m depth correspond to the known cavity. The other high-amplitude alignments labelled CH could be correlated with the presence of a channel. Slices from 1.9 to 2.5 m depth (Figure 9a) show two high-amplitude anomalies, A and C1. The first (A) comprises two parallel lines and could probably be related to traces of cart tracks. The second (C1) could be related to a cavity. Low reflection amplitude anomalies labelled V, V1, and V2 could be related to probable void spaces. It is possible to see an inversion of the polarity of the reflected electromagnetic wave in the correspondence of the anomaly V (Figure 9b). The polarity inversion could be due to the presence of a void (Conyers, 2015). The strange thing is that an increase in the amplitude of the reflected wave is expected in the presence of voids, while in this case, a low amplitude of the reflected wave is visible. A possible explanation could be that in these zones archaeologists report some channels of terracotta material covered in crushed bricks. These channels could be partially collapsed and filled with debris so that they would be small empty spaces.

The highest amplitudes were rendered into an isosurface (Conyers and Goodman, 1997; Conyers, 2004, 2012; Leucci, 2019, 2020; Giannino and Leucci, 2021). 3D amplitude isosurface rendering displays amplitudes of equal value in the GPR study volume. Shading usually illuminates these surfaces, making real archaeological structures appear. In this case, the threshold calibration is a delicate task to obtain valuable results. Figure 10 shows a virtual excavation at two different levels. It is possible to see the position of the anomalous zones well.

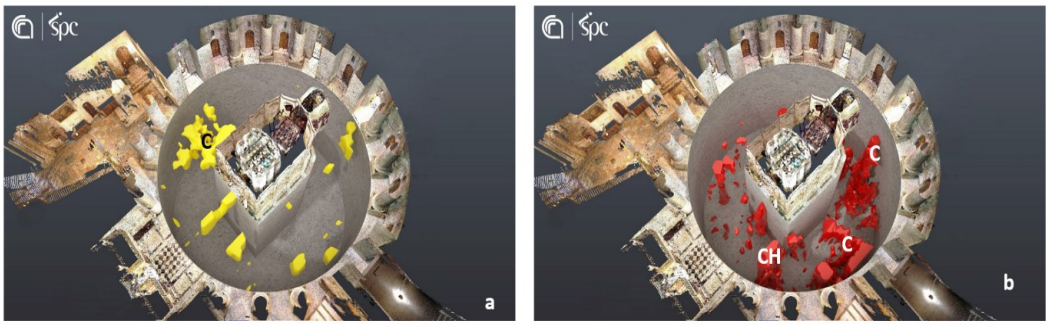

Figure 10. Isosurfaces in a virtual excavation: a) 0.6 m depth; b) 0.7 m depth.

Area RR+GG+FF

In this case, the time-slice technique has been used to display the amplitude variations within consecutive time windows of width Δt = 5 ns.

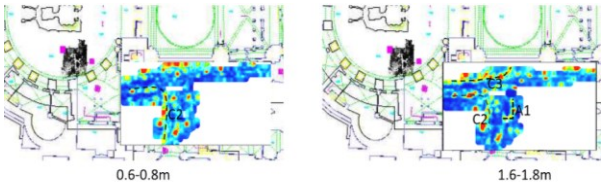

Figure 11. depth slices 0.6–1.8 m depth. C2 and C3: cavities; A1: walls.

In the slices ranging from 0.6 to 1.8 m depth (Figure 11), relatively high-amplitude alignments (labelled C2 and C3, respectively) are visible. These cavities, due to their shape, could be related to the presence of ancient channels. The deeper time slices (1.6–1.8 m) show other high-amplitude alignments (A1). They could be correlated to old structures of archaeological interest (walls).

Figure 12 shows the isosurface visualisation in a virtual excavation. Here, the position of the anomalous zones is visible. In this case, the anomalies labelled A1 are well evidenced. They are probably related to structures of archaeological interest.

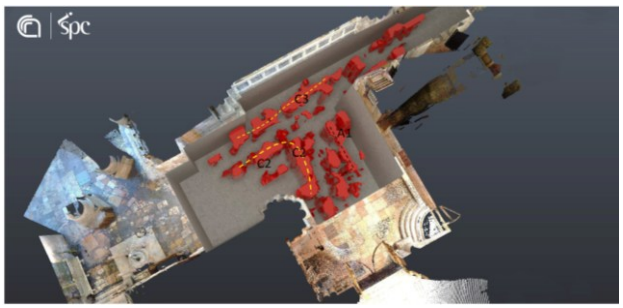

Figure 12. Isosurfaces in a virtual excavation: 1.6–1.8 m depth

Area AA+HH+II+LL+NN

In the slices ranging from 1.1 to 2.7 m depth (Figure 13), relatively high-amplitude alignments are visible. The anomalies labelled C4 could be associated with cavities (cisterns?). The anomaly A3 could be correlated to old structures (of archaeological interest).

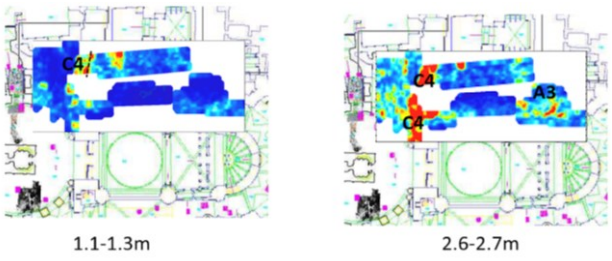

Figure 13. depth slices 0.0–0.8m deep. A3: structures; C4: cavity.

Figure 14 shows the isosurface visualisation in a virtual excavation. The position of the anomalous zones is visible. In this case, the anomalies labelled C4 and A3 are well evidenced.

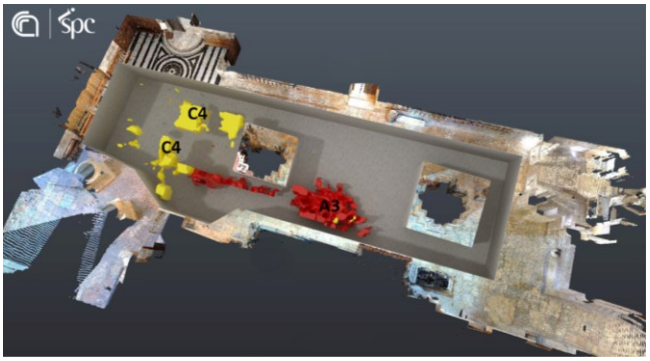

Figure 14. Isosurfaces in a virtual excavation: 1.0–2.7 m depth.

Area OO

In the slices ranging from 0.6 to 0.8 m depth (Figure 15), relatively high-amplitude alignments (labelled S) are visible. These could be related to underground services. The deeper time slice at 1.8–2.0 m depth (Figure 15) shows other high-amplitude alignments (A4). They could be correlated to old structures (archaeological interest).

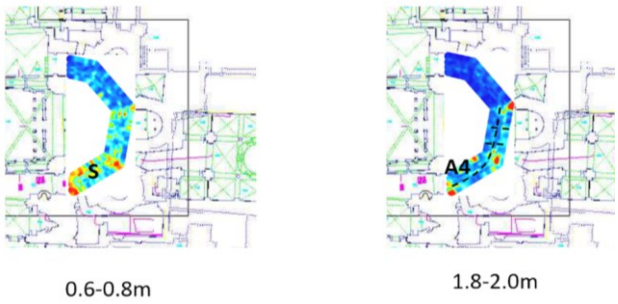

Figure 15. Depth slices 0.6–2.0 m deep. S: underground services; A4: archaeological structure.

Figure 16 shows the isosurface visualisation in a virtual excavation. Here, it is possible to see the spatial position of the anomaly labelled A4.

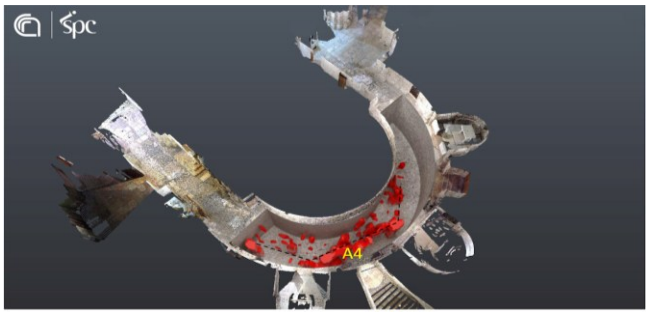

Figure 16. Isosurface in a virtual excavation: 1.0–1.8 m depth.

Area YY

Figure 17 shows the depth slices from 0.0 to 3.3 m. At depths between the anomalies CH2 and CH3 (Figure 17), at 0.7 and 0.8 m, probable channels are represented. The deeper time slice (1.0–1.1 m depth) shows other high-amplitude alignments (C5), which could be correlated to the presence of a large cavity.

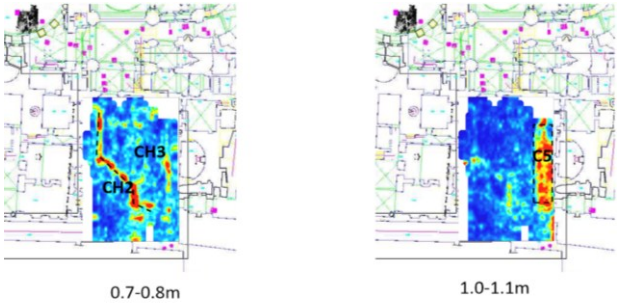

Figure 17. depth slices 0.7–1.1m depth (CH2 and CH3: channels; C5: cavity).

Figure 18 shows the isosurface visualisation in a virtual excavation. Here, the spatial positions of the CH2, CH3, and C5 anomalies can be seen.

A geostatistical analysis was performed using the GPR survey results to determine the depth of the bedrock inside the Basilica. Figure 19 shows the results. The depth of the bedrock (sacred rock) ranges from 0.2 m to 3.0 m.

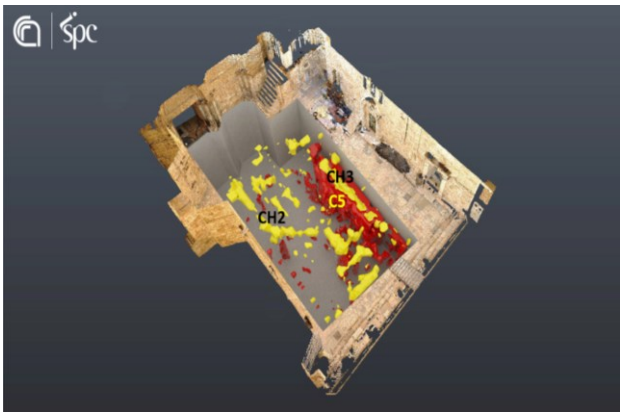

Figure 18. Isosurface in a virtual excavation.

The 900 MHz data analysis

Figure 20 shows the results for the 900 MHz antenna. The reflection event, evidenced by a dashed yellow line, is probably related to the thickness of the paving, which ranges from 0.18 to 0.22 m. Below the paving, an inhomogeneous ground fill (small stones, etc.) can be seen. Other reflection events (labelled 'S') are visible at depths between 0.3 and 0.4 m. They are probably related to the presence of pipes.

The EM-wave velocity plays an important role in defining shallow subsurface water content. Numerous studies have used GPR techniques to determine subsurface moisture (Annan et al., 1990; Du and Rummel, 1994; Mellet, 1995; Grandjean et al., 2000; Leucci, et al., 2002). However, since each technique is generally considered individually and is efficient only in a specific context, it is not easy to compare the results because of different field conditions. The dielectric constant (K) for pure water is about 80, whereas it varies between 4 and 10 for most dry geological material. If only a small amount of water is contained in the material, the value of K will increase considerably and, conversely, the EM-wave velocity will decrease significantly. Thus, K is a good measure of the water content in the ground. Several formulae have been developed theoretically and empirically to give the dielectric response of heterogeneous mixtures such as water-saturated soils.

Figure 19. The bedrock depth inside the Basilica, rendered using isoipse.

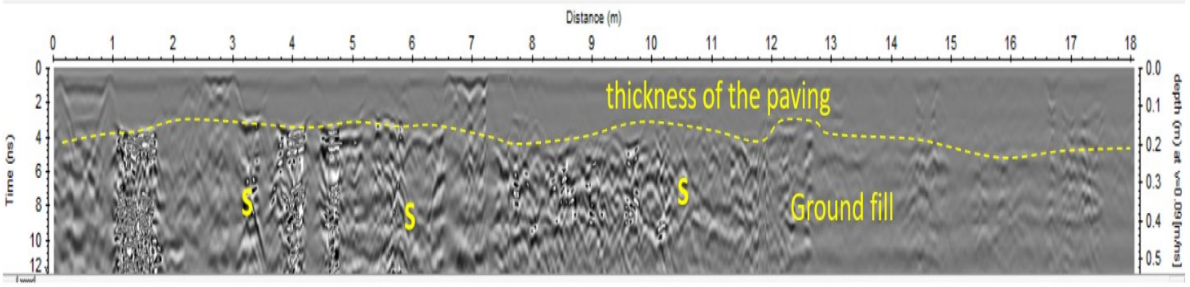

Figure 20. Processed GPR sections related to the 900 MHz antenna.

One such formula is the complex refractive index method (CRIM) equation, which is often used to interpret EM logging data (Greaves et al., 1996). The major problem with the CRIM formula is that it does not consider the geometrical information about the internal structure of rocks and the microscopic fluid distribution. This significantly affects the dielectric properties of partially saturated rocks (Endrea and Knight, 1992). The above restriction may be overcome by using the Hanai–Bruggeman formula (Endrea and Knight, 1992). The main problem with the two previous approaches is that it is impossible to derive both the porosity and the water content from the dielectric constant. Therefore, obtaining information about the water content without strong a priori assumptions is impossible. For this reason, it is preferable to use the well-known empirical equation, derived by Topp et al. (1980), relating the dielectric response K of various soil samples (with different degrees of saturation) to their net water content, w. This formula is given by:

$$w = -5.3 \times 10^{-2} + 2.92 \times 10^{-2}(K) - 5.5 \times 10^{-4}(K)^2 + 4.3 \times 10^{-6}(K)^3 \quad (1)$$

This equation was nearly independent of soil texture, bulk density, temperature and salinity (Du and Rummel 1994). Here, the volumetric water content was determined from the dielectric properties of subsurface material, using the above empirical relationship (1). The EM-wave velocity can be estimated from GPR data in several ways (Conyers and Goodman 1997; Huisman et al., 2003); the conventional methods involve common depth point (CDP) and wide-angle reflection and refraction (WARR) datasets. Both methods require two antennae in separate units and relatively long acquisition times. In the first case, both antennae are simultaneously moved apart on either side of the midpoint of the profile. In the second case, the position of one antenna is fixed while the other is moved along the profile direction.

The EM wave velocity can be more quickly and easily determined from the reflection profiles acquired in continuous mode, using the characteristic hyperbolic reflection shape from a point source (Fruhwirth et al., 1996). This is a prevalent method of velocity estimation, and it is based on the phenomenon that a small object reflects EM-waves in almost every direction. In the dataset, several hyperbolic reflections caused by stones and objects of small dimensions (Figure 21) are present, enabling EM wave velocity analysis to be performed. Figure 21 shows an example of velocity analysis performed on the data set.

The EM wave velocity analysis allows for estimating the volumetric water content related to the subsoil (Figure 22). Figure 22c shows the 2D distribution of the volumetric water content. Values range between 12 and 27%. The dashed black lines show a probable area of rising damp, in which the volumetric water content values range from 20 to 27%. Dashed dark arrows indicate a probable rise in humidity from the subsoil.

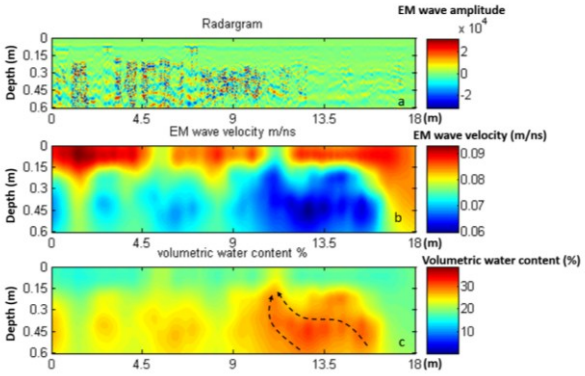

Figure 22. a) Processed GPR sections related to 900 MHz antenna; b) EM wave velocity distribution; c) volumetric water content distribution.

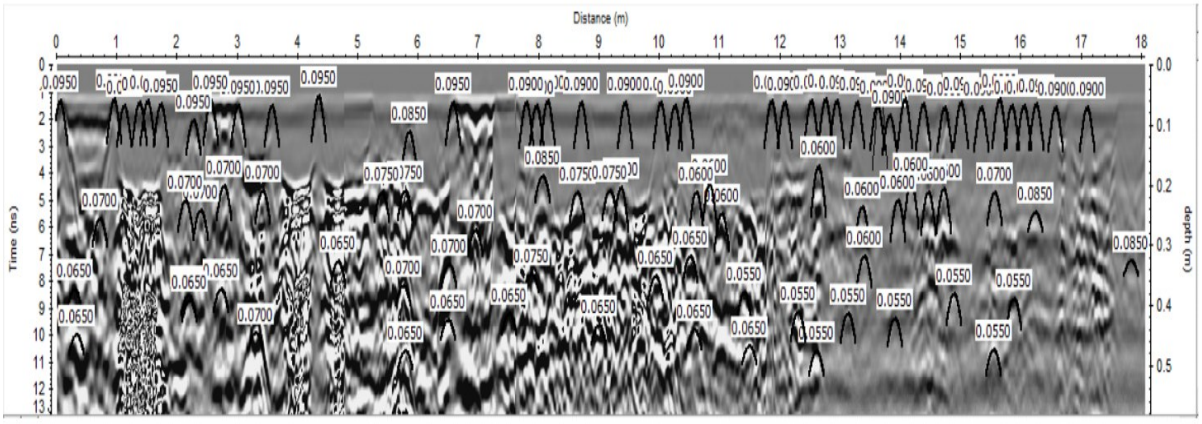

Figure 21. Processed GPR sections related to 900 MHz antenna: EM wave velocity analysis.

CONCLUSIONS

The GPR results are encouraging. They demonstrate the potential of the GPR method in the context of the Church of the Holy Sepulchre. The data allowed evidence of the bedrock's depth (sacred rock), which ranges from 0.3 to 2.5 m. The paving thickness varies from 0.15 to 0.45 m. The GPR survey highlighted various structures of probable archaeological interest.

Several anomalies were found in the roundabout. Some of these, labelled C in Figures 9, 10 and 13, were attributable to already-known cavities. The anomalies labelled A and C1 (Figure 11) seem to be interesting because they reveal probable carriage tracks (A) and a cavity (C1).

Furthermore, Padre Corbo (1981) documented a channel (CH in Figures 10 and 13) in the excavation. In all the remaining investigated areas, the results of the GPR investigation highlight the presence of strong canalisation (the anomalies indicated with CH) with probable water collection areas (cisterns). Wall structures are also identified (A1 to A4).

The volumetric water content data shows a subsoil with a high concentration of humidity (20–30%), suggesting a rise from the bottom upwards (Figure 23).

Archaeological excavations undertaken after these geophysical investigations confirmed the Roman road near the *aedicule* (anomaly A) and some wall structures (A1). The bedrock depth and thickness of the paving were also confirmed.

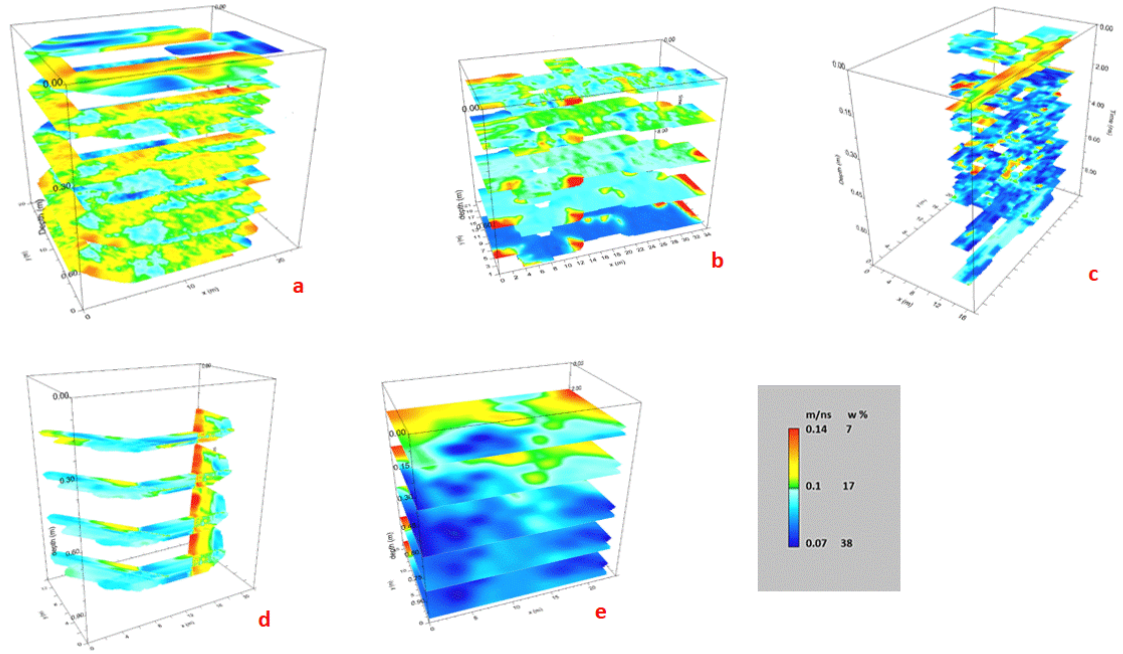

Figure 23. Water content: a) Area B+C+D+E; b) area A+H+I+L+M+N; c) area F+G+R; d) area O+P+Q; e) area Y.

DISCLOSURE STATEMENT

The authors declare no conflict of interest.

REFERENCES

Alexakis, E., Delegou, E.T., Lampropoulos, K.C., Apostolopoulou, M., Ntoutsi, I. and Moropoulou, A. (2018). NDT is a monitoring tool for the work's progress and the assessment of materials and rehabilitation interventions at the Holy Aedicule of the Holy Sepulchre. *Construction and Building Materials* 189, 512–526

Annan, A.P. and Davis, J.L. (1978). Methodology for radar transillumination experiments: Report of activities. *Geological Survey of Canada, Paper* 78-1B: 107–110.

Annan, A.P., Scaife, J.E. and Giamou, P. (1990). Mapping buried barrels with magnetics and ground penetrating radar. 60th SEG Meeting, San Francisco, USA, Expanded Abstracts, 422–423.

Conyers, L.B. (2004). Moisture and soil differences are related to the spatial accuracy of amplitude maps at two archaeological test sites. *Proceedings of the Tenth International Conference on Ground Penetrating Radar*. Delft, The Netherlands, June 21–24, 2004.

Conyers, L.B. (2006). Innovative ground-penetrating radar methods for archaeological mapping. *Archaeological Prospection* 13 (2): 139–141.

Conyers, L.B., (2012). *Interpreting ground-penetrating radar for archaeology*. Left Coast Press, Walnut Creek

Conyers, L.B. (2015). Analysis and interpretation of GPR datasets for integrated archaeological mapping. *Near Surface Geophysics* 13, 1–7

Conyers, L.B. and Goodman, D. (1997). *Ground-penetrating radar: An introduction for archaeologists*. AltaMira Press, Walnut Creek, California.

Corbo, V.C. (1981). *Il Santo Sepolcro Di Gerusalemme: Aspetti Archeologici Dalle Origini Al Periodo Crociato*. Franciscan Printing Press, Jerusalem.

De Giorgi, L., Barbolla, D.F., Ferrari, I., Giuri, F., Torre, C. and Leucci, G., (2023a). Geophysical Investigation at the Santa Chiara Church in Nardò (Southern Italy). *Heritage* 6 (3): 2978–2989. https://doi.org/10.3390/heritage6030158

De Giorgi, L., Comisi, F., Barbolla, D.F., Longhitano, L., Torre, C. and Leucci, G. (2023b). The Basilica of Santa Croce (Lecce- Italy): study the conservation state by ground-penetrating radar and electrical resistivity tomography. *Exploration Geophysics* 55 (1): 15–25. https://doi.org/10.1080/08123985.2023.2251520

Du, S. and Rummel, P. (1994). Reconnaissance studies of moisture in the subsurface with GPR. Proceedings of the 5th International Conference on Ground Penetrating Radar, Kitchener, Ontario, Canada: 1224–1248.

Endrea, A.L. and Knight, R. (1992). A theoretical treatment of the effect of microscopic fluid distribution on the dielectric properties of partially saturated rocks. *Geophysical Prospecting* 40, 307–324.

Fruhwirth, R.K., Schmoller, R. and Oberaigner, E.R. (1996). Some aspects of the estimation of electromagnetic wave velocities. Proceedings of the 6th International Conference on Ground Penetrating Radar, Tohoku University, Sendai, Japan: 135–138.

Giannino, F. and Leucci, G., (2021). *Electromagnetic methods in geophysics: Applications in GeoRadar, FDEM, TDEM, and AEM*. Wiley: 352p. ISBN: 978-1-119-77098-5

Goodman, D., Piro, S., Nishimura, Y., Patterson, H. and Vince G. (2004). Discovery of a 1st century AD Roman amphitheatre and other structures at the Forum Novum by GPR. *Journal of Environmental and Engineering Geophysics* 9: 35–42.

Goodman, D., Steinberg, J., Damiata, B., Nishimure, Y., Schneider, K., Hiromichi, H and Hisashi, N. (2006). GPR overlay analysis for archaeological prospection. Proceedings of the 11th International Conference on Ground Penetrating Radar, Columbus, Ohio; CD-ROM.

Grandjean, G., Gourry, J.C. and Bitri, A. (2000). Evaluation of GPR techniques for civil-engineering applications: study on a test site. *Journal of Applied Geophysics* 45, 141–156.

Greaves, R.J., Lesmes, D.P., Lee, J.M. and Toksöz, N. (1996). Velocity variations and water content estimated from multi-offset, ground-penetrating radar. *Geophysics* 61, 683–695.

Huisman, J.A., Hubbard, S.S., Redman, J.D. and Annan, A.P. (2003). Measuring soil water content with ground penetrating radar: A review. *Vadose Zone Journal* 2, 476–491.

Lampropoulos, K.C., Moropoulou, A. and Korres, M. (2017). Ground penetrating radar prospection of the construction phases of the Holy Aedicula of the Holy Sepulchre in correlation with architectural analysis. *Construction and Building Materials* 155: 307–322

Leckebusch, J. (2003). Ground-penetrating radar: A modern three-dimensional prospection method. *Archaeological Prospection* 10: 213–240.

Leucci, G. (2008). Ground penetrating radar: the electromagnetic signal attenuation and maximum penetration depth, *Scholarly Research Exchange* 2008, article ID 926091. https://doi.org/10.3814/2008/926091.

Leucci G. (2015). Geofisica Applicata all'Archeologia e ai Beni Monumentali. Dario Flaccovio Editore, Palermo, 368p. ISBN: 9788857905068

Leucci, G. (2019), *Nondestructive testing for archaeology and cultural heritage: A practical guide and new perspective*. Springer editore, 217p. ISBN 978-3-030-01898-6

Leucci, G. (2020). *Advances in geophysical methods applied to forensic investigations: New developments in acquisition and data analysis methodologies*. Springer editore, 200p. ISBN 978-3-030-46241-3

Leucci, G., Cataldo, R. and De Nunzio, G. (2007). Assessment of fractures in some columns inside the crypt of the Cattedrale di Otranti using integrated geophysical methods. *Journal of Archaeological Sciences* 34 (2): 222–32.

Leucci, G. and De Giorgi, L. (2022). Integrated NDT for building cultural heritage. In *Handbook of Cultural Heritage Analysis*: 739–769. ISBN 978-3-030-60015-0

Leucci, G., Negri, S., Carrozzo, M.T. and Nuzzo, L. (2002). Use ground penetrating radar to map subsurface moisture variations in an urban area. *Journal of Environmental and Engineering Geophysics* 7 (2), 69–77.

Moropoulou, A., Labropoulos, K.C., Delegou, E.T., Karoglou, M. and Bakolas, A. (2013). Non-destructive techniques as a tool for the protection of built cultural heritage. *Construction and Building Materials* 48, 1222–1239

Moropoulou, A.I., Labropoulos, K.C. and Katsiotis, N.S. (2012). Ground penetrating radar is used to assess the decay state of Hagia Sophia's mosaics. In Paipetis, A.S., Matikas, T.E., Aggelis, D.G. and Van Hemelrijck, D. eds. *Emerging technologies in non-destructive testing*. V. Balkema: Taylor & Francis Group: 25–30.

Moropoulou, A., Zacharias, N., Delegou, E.T., Apostolopoulou, M., Palamara, E. and Kolaiti, A. (2018). OSL mortar dating to elucidate the construction history of the Tomb Chamber of the Holy Aedicule of the Holy Sepulchre in Jerusalem. *Journal of Archaeological Science: Reports* 19: 80–91

Riminesi, C., Manganelli Del Fà, R., Brizzi, S., Rocco, A., Fontana, R., Bertasa, M., Grifoni, E., Impallaria, A., Leucci, G., De Giorgi, L., Ferrari, I., Giuri, F., Penoni, S. and Felici, A. (2024). Architectural assessment of wall paintings using a multimodal and multi-resolution diagnostic approach: The test site of the Brancacci chapel in Firenze. *Journal of Cultural Heritage* 66: 99–109. https://doi.org/10.1016/j.culher.2023.11.012

Tanasi, D., Lanteri, R., Hassam, S., Trapani, P., Calderone, D., Kingsland, K., De Giorgi, L., Ferrari, I., Fragalá, G., Giuri, F. and Leucci, G., (2023). Remote sensing campaign at the Roman villa of Caddeddi on the Tellaro river (Noto, Italy). *Exploration Geophysics* 55 (1). https://doi.org/10.1080/08123985.2023.2266446.

Topp, G.C., Davis, J.L. and Annan, A.P. (1980). Electromagnetic determination of soil water content: measurements in coaxial transmission lines. *Water Resources Research* 16 (3), 574–582.